**NANO EXPRESS**　　　　　　　　　　　　　　　　　　**Open Access**

# Thermal conductivity in porous silicon nanowire arrays

Jeffrey M Weisse[1], Amy M Marconnet[1], Dong Rip Kim[1], Pratap M Rao[1], Matthew A Panzer[2], Kenneth E Goodson[1] and Xiaolin Zheng[1*]

## Abstract

The nanoscale features in silicon nanowires (SiNWs) can suppress phonon propagation and strongly reduce their thermal conductivities compared to the bulk value. This work measures the thermal conductivity along the axial direction of SiNW arrays with varying nanowire diameters, doping concentrations, surface roughness, and internal porosities using nanosecond transient thermoreflectance. For SiNWs with diameters larger than the phonon mean free path, porosity substantially reduces the thermal conductivity, yielding thermal conductivities as low as 1 W/m/K in highly porous SiNWs. However, when the SiNW diameter is below the phonon mean free path, both the internal porosity and the diameter significantly contribute to phonon scattering and lead to reduced thermal conductivity of the SiNWs.

**Keywords:** Thermal conductivity, Silicon nanowires, Porous silicon, Thermoreflectance

## Background

Silicon with a high density of nanoscale features such as interfaces, porosity, and impurities can have thermal conductivities ($\kappa$) up to three orders of magnitude lower than that of bulk Si through enhanced phonon scattering [1-17]. For example, the thermal conductivity of nanoporous bulk Si generally decreases with increasing porosity and decreasing pore size [1-9] and, with high porosity, approaches the amorphous limit (0.2 to 0.5 W/m/K) [1-3]. Similarly, silicon nanowires (SiNWs) with diameters significantly smaller than the bulk phonon mean free path ($\Lambda \approx 100$ to 300 nm at 300 K) were reported to have thermal conductivity values as low as 0.76 W/m/K due to strong phonon scattering at the SiNW boundary [10,11]. Introducing surface roughness to the SiNWs leads to additional phonon scattering at length scales even smaller than the NW diameter [12-16]. However, there have been few investigations on the combined effects of external dimensions and internal porosity on the thermal conductivity values of SiNWs. In this work, we report the effects of internal porosity on the thermal conductivity of SiNWs of two different

diameters that allow the phonon propagation to span the range from ballistic to diffusive thermal transport ($d_{avg} \approx 350$ and 130 nm) by measuring the thermal conductivity of vertically aligned SiNW arrays using nanosecond transient thermoreflectance (TTR). As opposed to measurements of individual SiNWs, measurements of arrays of SiNWs offer the advantage of averaging out the inherent thermal conductivity variations that are caused by differences in SiNW diameter, surface roughness, and defects within the arrays.

## Methods

The vertically aligned SiNW arrays are fabricated using a four-step preparation process illustrated in Figure 1. Two sets of vertically aligned SiNW arrays with different diameters are fabricated (Figure 1a,e) using top-down etching techniques to achieve a range of porosities (Table 1). For the first set, the diameter ($d_{avg} \approx 300$ to 350 nm) and density of the SiNWs are controlled by nanosphere lithography [18]. Specifically, a monolayer of $SiO_2$ spheres is deposited using the Langmuir-Blodgett method onto Si wafers (p-type with boron dopant atoms, (100)) and used as a mask for the subsequent etching steps. The internal porosity of the SiNWs is varied from nonporous to highly porous by changing the etching methods and conditions [19-21]. Nonporous SiNWs are

* Correspondence: xlzheng@stanford.edu
[1]Department of Mechanical Engineering, Stanford University, Stanford, CA 94305, USA
Full list of author information is available at the end of the article
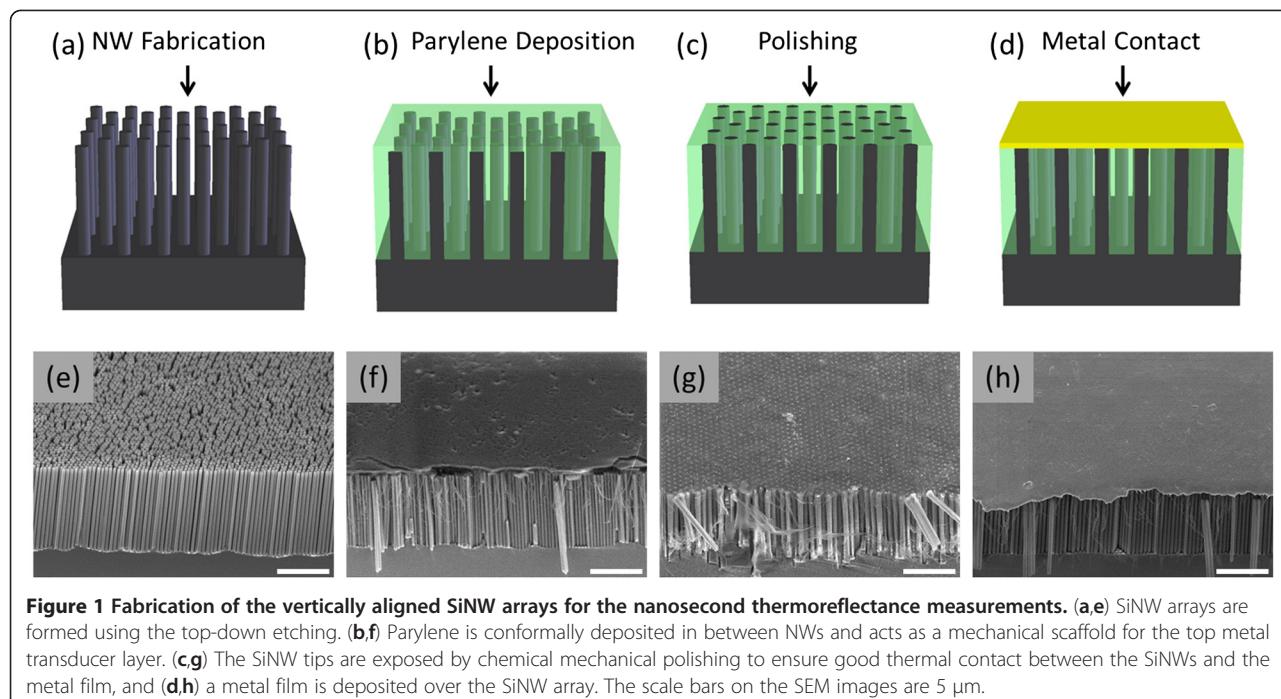
**Figure 1 Fabrication of the vertically aligned SiNW arrays for the nanosecond thermoreflectance measurements. (a,e)** SiNW arrays are formed using the top-down etching. **(b,f)** Parylene is conformally deposited in between NWs and acts as a mechanical scaffold for the top metal transducer layer. **(c,g)** The SiNW tips are exposed by chemical mechanical polishing to ensure good thermal contact between the SiNWs and the metal film, and **(d,h)** a metal film is deposited over the SiNW array. The scale bars on the SEM images are 5 μm.

formed by deep reactive ion etching (DRIE), and the resulting SiNWs have slightly smaller diameters ($d_{avg} \approx$ 300 nm) than the spheres used as the etch mask [22]. Porous SiNW arrays are fabricated by metal-assisted chemical etching (MACE) in a solution of 4.8 M HF and 0.3 M $H_2O_2$, and the porosity is controlled by varying the metal catalyst and wafer doping concentrations [19-21,23-25]. For low-porosity nanowires, the catalyst layer consists of a 15-nm Ag film covered by 5-nm Au, while for the moderate to highly porous nanowires, a 50-nm Ag film is used as the catalyst and the initial wafer doping concentration is varied. The second set of SiNWs, with generally smaller diameters, is fabricated using a two-step MACE process with silver salts [19,20,23,26,27]. First, the Ag film is deposited using a

solution of 0.005 M $AgNO_3$ and 4.8 M HF for 1 min. Then, the SiNWs are formed by etching in a solution of 4.8 M HF with various concentrations of $H_2O_2$ (0.15, 0.30, 0.60, and 1.20 M) to adjust the SiNW porosity [19,20,23,26,27]. The resulting SiNWs have an average diameter of 130 nm, but there is significant diameter variation within the SiNW array ($d \approx$ 20 to 300 nm). For all the samples, the SiNW length is approximately 10 μm.

Following the formation of the SiNW arrays, the gaps between SiNWs are completely filled with parylene N (poly-para-xylylene; Figure 1b,f), which has a thermal conductivity significantly lower than the SiNWs ($K_{parylene}$ = 0.125 W/m/K) and a high melting temperature ($T_m \approx$ 410°C). The parylene filling quality is inspected by examining multiple freshly cut cross sections under a scanning electron microscope (SEM), and no parylene voids are observed. The SiNW tips are subsequently exposed via chemical mechanical polishing to remove the parylene covering the SiNWs (Figure 1c,g) that facilitates the SiNWs to form a good thermal contact with the top metal film. Finally, a 15-nm Cr layer (for adhesion) and a 500-nm Cu layer are deposited by electron beam evaporation on top of the SiNW tips to form a flat, reflective transducer layer for the thermoreflectance measurements (Figure 1d,h).

The thermal conductivity of the vertical SiNW arrays is measured at room temperature by nanosecond TTR; the details of which can be found in Panzer et al. [28]. Briefly, the metal transducer layer that is deposited on the parylene-filled SiNW array is heated by a 3-mm

**Table 1 Summary of SiNW arrays with varied diameters and porosities**

|  | Diameter control | Porosity control |
| --- | --- | --- |
| Set 1 | Nanosphere lithography | Etching method and doping concentration |
|  | $d_{avg} \approx$ 300 to 350 nm | Nonporous: DRIE |
|  | $VF_{DRIE}$ = 21% to 23% | Low porosity: Ag/Au MACE |
|  | $VF_{MACE}$ = 45% to 60% | Moderate porosity: Ag MACE, lightly doped |
|  |  | High porosity: Ag MACE, heavily doped |
| Set 2 | Silver salts | MACE etchant solution |
|  | $d_{avg} \approx$ 130 nm | Low porosity, 0.15 M $H_2O_2$ |
|  | VF = 26% to 35% | High porosity, 1.2 M $H_2O_2$ |

diameter, 532-nm wavelength, 6-ns pulse from a Nd:
YAG laser at a frequency of 10 Hz. The reflected inten-
sity of the probe laser ($d \approx 20$ μm, 10 mW, 658 nm,
continuous wave) is directly correlated to the
temperature of the metal layer that is affected by the
thermal conductivity of the SiNW/parylene composite.
The thermal conductivity of the SiNW/parylene com-
posite and its interface thermal resistance at the top
metal layer are extracted using a two-parameter fit of
the measured temperature decay trace (normalized by the
maximum temperature) to the solution of a one-
dimensional heat diffusion equation for a multilayer stack
with surface heating. The volumetric heat capacity of the
film ($C_{v,composite}$) is assumed to be the volumetric average
of the heat capacity of parylene ($C_{v,parylene}$) and bulk sili-
con ($C_{v,Si}$): $C_{v,composite} = VF \cdot C_{v,Si} + (1 - VF) \cdot C_{v,parylene}$,
where VF is the volume fraction of SiNWs within the
composite. The VF of SiNWs within each array is mea-
sured directly from top-view SEM images of the film by
setting a brightness threshold to define the edge of
SiNWs. The average thermal conductivity of an individual
SiNW within the array is calculated from the extracted
film thermal conductivity ($K_{composite}$) using an effective
medium model: $K_{NW} = [K_{composite} - (1 - VF)K_{parylene}]/VF$,
where $K_{NW}$ and $K_{parylene}$ are the thermal conductivities of
the SiNWs and parylene, respectively. In this model,
SiNW arrays are treated as thermal resistors in parallel
with the parylene matrix. The uncertainty of the extracted
$k_{NW}$ is calculated through an error propagation analysis
given by the following equation:

$$\Delta k_{NW} = \sqrt{\left(\frac{\partial k_{NW}}{\partial k_{film}} \Delta k_{film}\right)^2 + \left(\frac{\partial k_{NW}}{\partial VF} \Delta VF\right)^2 + \left(\frac{\partial k_{NW}}{\partial k_{parlyene}} \Delta k_{parlyene}\right)^2}$$

(1)

where $\Delta k_{parylene}$ is the thermal conductivity variation
from the literature. $\Delta k_{film}$ and $\Delta VF$ are the measured
spot-spot variation in the same type of samples. Detailed
error analysis data for all the data reported here can be
found in Additional file 1.

## Results and discussion

The thermal conductivity for the SiNWs with large dia-
meters ($d_{avg} \approx 300$ to 350 nm) demonstrates a clear de-
crease with increasing porosity (Figure 2). The thermal
conductivity of nonporous SiNWs, though with rough
surfaces, is 142 ± 13 W/m/K, which is very close to that
of bulk Si ($\kappa \approx 150$ W/m/K). This suggests that for
large-diameter SiNWs, surface roughness at this depth
and periodicity does not cause effective phonon-external
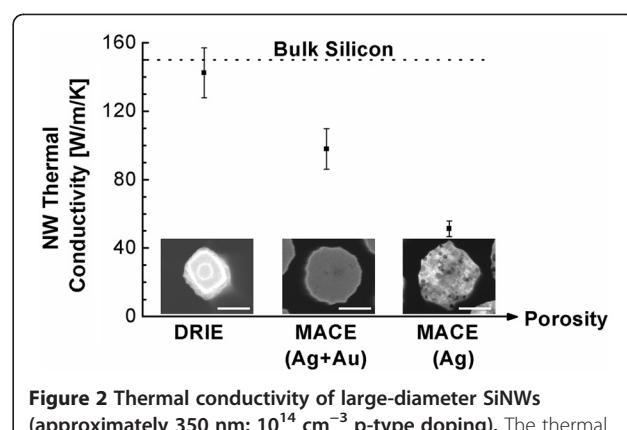


**Figure 2 Thermal conductivity of large-diameter SiNWs
(approximately 350 nm; $10^{14}$ cm$^{-3}$ p-type doping).** The thermal
conductivity with three levels of porosity, corresponding to different
etching conditions, is shown. The thermal conductivity decreases
significantly with increasing porosity. The inset images show the top
view of the SiNWs, and the scale bars are 200 nm.

boundary scattering and therefore has little effect on the
thermal conductivity. On the other hand, the internal
porosity of SiNWs significantly reduces the thermal con-
ductivity from 142 W/m/K for the nonporous SiNWs to
98 W/m/K (Au/Ag-MACE) and 51 W/m/K (Ag-MACE)
for the increasingly porous SiNWs.

The thermal conductivity of large-diameter SiNW
arrays ($d_{avg} \approx 350$ nm) with three different p-type boron
dopant atom concentrations ($10^{14}$, $10^{16}$, and $10^{18}$ cm$^{-3}$)
is further investigated for both nonporous and porous
NWs (Figure 3). The thermal conductivity of nonpor-
ous SiNWs decreases slightly with increasing doping
concentration due to the increased phonon-impurity
scattering, similar to bulk Si [29,30]. Conversely, the
thermal conductivity of porous SiNWs drops to about
1 W/m/K when the doping concentration is increased
from $10^{16}$ to $10^{18}$ cm$^{-3}$. It should be noted that the
main reason for the dramatic drop in conductivity
with doping concentration is that higher doping con-
centrations lead to increased porosity in SiNWs fabri-
cated with MACE (Figure 3b,c,d). The dopant atom
sites act as preferred locations for pore formation
[19,23,26,27]. In comparison to the internal NW por-
osity, the phonon-impurity scattering at higher doping
concentration has a much smaller impact on the ther-
mal conductivity [2,12].

The thermal conductivities of SiNWs with small dia-
meters ($d_{avg} \approx 130$ nm) also decrease with increasing
porosity (Figure 4), similar to the large-diameter SiNWs.
However, the thermal conductivity of these SiNWs is
much smaller than that of large-diameter SiNWs of
similar porosities (i.e., the same etchant solution, 0.3 M
$H_2O_2$). Specifically, the thermal conductivity is reduced
from 51 W/m/K for the large-diameter ($d_{avg} \approx 350$ nm)
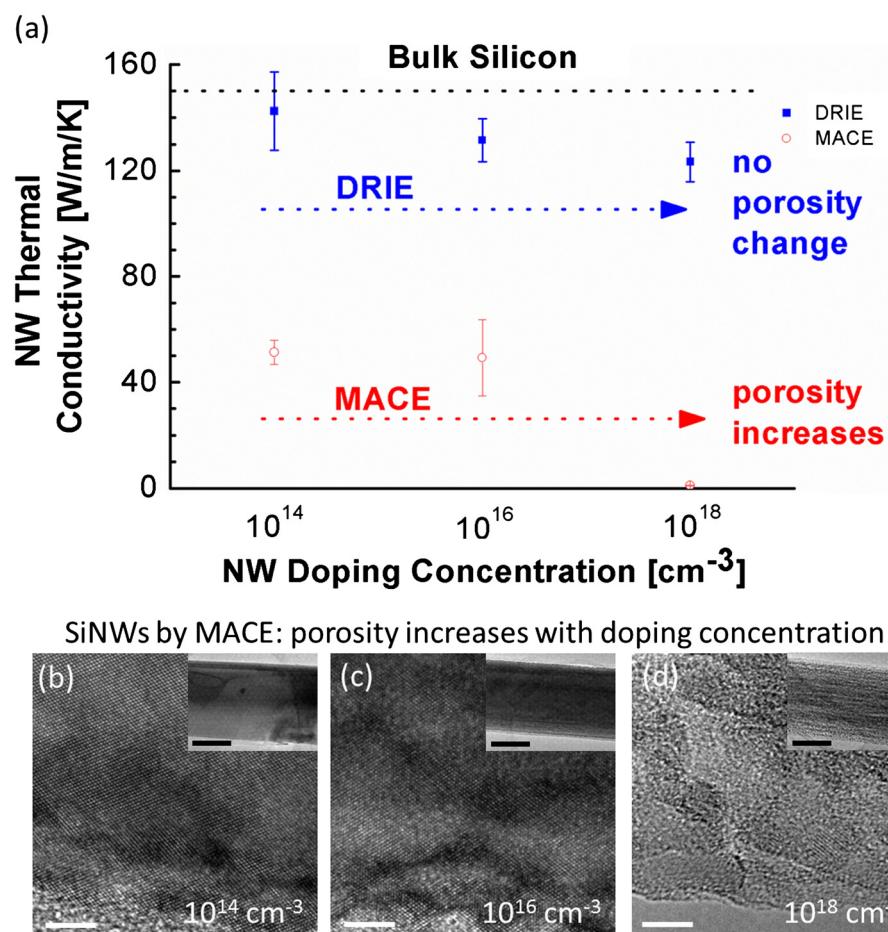
**Figure 3 Thermal conductivity of large-diameter nonporous and porous SiNW arrays.** (**a**) Thermal conductivity of nonporous and porous SiNW arrays of large diameters as a function of doping concentrations. TEM images show the relative porosity for Ag-MACE SiNW arrays fabricated with doping concentrations of (**b**) $10^{14}$, (**c**) $10^{16}$, and (**d**) $10^{18}$ cm$^{-3}$. The scale bars on the TEM and inset TEM images are 5 and 200 nm, respectively. The uncertainty bar for the MACE nanowires with a doping concentration of $10^{18}$ cm$^{-3}$ is on the order of the data point marker size.

SiNWs to 28 W/m/K for the smaller-diameter SiNWs ($d_{avg} \approx 130$ nm). This highlights the significant impact of phonon-external boundary scattering on the thermal conductivity at length scales that are smaller than the phonon mean free path. The additional reduction in thermal conductivity (to 17 W/m/K) with increasing $H_2O_2$ concentration for the smaller-diameter SiNWs indicates that the increasing internal porosity also has a significant impact on the thermal conductivity.

## Conclusions

In summary, we measured the thermal conductivity of SiNW arrays with various nanowire diameters, doping concentrations, surface roughness and internal porosities using a nanosecond transient thermoreflectance method. When the SiNW diameter ($d_{avg} \approx 350$ nm) is larger than the phonon mean free path in the bulk silicon, the thermal conductivity shows little dependence on the doping
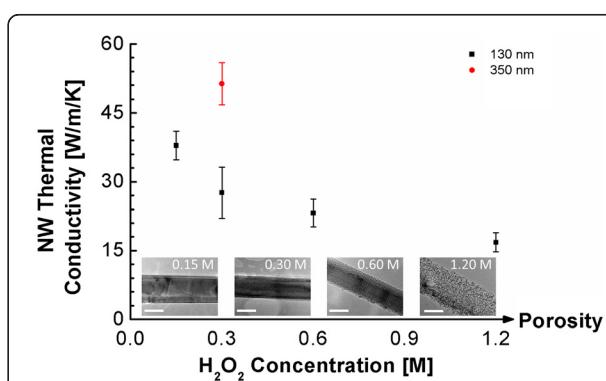


**Figure 4 Thermal conductivity of small-diameter (approximately 130 nm) SiNWs ($10^{14}$ cm$^{-3}$) as a function of porosity.** For comparison, the thermal conductivity of the large-diameter SiNW etched at the same condition is shown as the red circle. Increasing nanowire porosity is realized by increasing the $H_2O_2$ concentration during MACE, as evidenced by the inset TEM images. The scale bars on all the TEM images are 100 nm.

concentration and surface roughness but decreases significantly with increasing porosity due to phonon scattering at the pore interfaces. In contrast, when the SiNW diameter ($d_{avg} \approx 130$ nm) is smaller than the phonon mean free path, the thermal conductivity strongly depends on both the external boundary-phonon scattering and the internal pore interface-phonon scattering, leading to a significant reduction in the thermal conductivity for small-diameter SiNWs.

## Additional file

**Additional file 1: Error analysis of the thermal conductivity of vertical SiNW arrays.** An XLSX file showing detailed error analysis data for all the data reported.

## Competing interests

The authors declare that they have no competing interests.

## Authors' contributions

JMW, AMM, KEG, and XLZ designed and interpreted the experiments. JMW and DRK fabricated the samples. JMW and PMR performed SEM and TEM characterization. AMM and MAP designed and carried out the thermoreflectance setup and measurements. All authors contributed to and approved the final manuscript.

## Author details

[1]Department of Mechanical Engineering, Stanford University, Stanford, CA 94305, USA. [2]KLA-Tencor Corporation, Milpitas, CA 95035, USA.

## References

1. Gesele G, Linsmeier J, Drach V, Fricke J, Arens-Fischer R: **Temperature-dependent thermal conductivity of porous silicon.** *J Phys D: Appl Phys* 1997, **30**:2911–2916.
2. Yang CC, Li S: **Basic principles for rational design of high-performance nanostructured silicon-based thermoelectric materials.** *ChemPhysChem* 2011, **12**:3614–3618.
3. Miyazaki K, Tanaka S, Nagai D: **Heat conduction of a porous material.** *J Heat Transfer* 2012, **134**:051018.
4. Alvarez FX, Jou D, Sellitto A: **Pore-size dependence of the thermal conductivity of porous silicon: a phonon hydrodynamic approach.** *Appl Phys Lett* 2010, **97**:033103.
5. de Boor J, Kim DS, Ao X, Hagen D, Cojocaru A, Foell H, Schmidt V: **Temperature and structure size dependence of the thermal conductivity of porous silicon.** *Europhys Lett* 2011, **96**:16001.
6. Gomes S, David L, Lysenko V, Descamps A, Nychyporuk T, Raynaud M: **Application of scanning thermal microscopy for thermal conductivity measurements on meso-porous silicon thin films.** *J Phys D: Appl Phys* 2007, **40**:6677–6683.
7. He Y, Donadio D, Lee J-H, Grossman JC, Galli G: **Thermal transport in nanoporous silicon: interplay between disorder at mesoscopic and atomic scales.** *ACS Nano* 2011, **5**:1839–1844.
8. Lee J-H, Galli GA, Grossman JC: **Nanoporous Si as an efficient thermoelectric material.** *Nano Lett* 2008, **8**:3750–3754.
9. Romano G, Di Carlo A, Grossman JC: **Mesoscale modeling of phononic thermal conductivity of porous Si: interplay between porosity, morphology and surface roughness.** *J Comput Electron* 2012, **11**:8–13.
10. Boukai AI, Bunimovich Y, Tahir-Kheli J, Yu JK, Goddard WA, Heath JR: **Silicon nanowires as efficient thermoelectric materials.** *Nature* 2008, **451**:168–171.
11. Li DY, Wu YY, Kim P, Shi L, Yang PD, Majumdar A: **Thermal conductivity of individual silicon nanowires.** *Appl Phys Lett* 2003, **83**:2934–2936.
12. Hochbaum AI, Chen RK, Delgado RD, Liang WJ, Garnett EC, Najarian M, Majumdar A, Yang PD: **Enhanced thermoelectric performance of rough silicon nanowires.** *Nature* 2008, **451**:163–167.
13. Lim J, Hippalgaonkar K, Andrews SC, Majumdar A, Yang P: **Quantifying surface roughness effects on phonon transport in silicon nanowires.** *Nano Lett* 2012, **12**:2475–2482.
14. Liu L, Chen X: **Effect of surface roughness on thermal conductivity of silicon nanowires.** *J Appl Phys* 2010, **107**:033501.
15. Luisier M: **Investigation of thermal transport degradation in rough Si nanowires.** *J Appl Phys* 2011, **110**:074510.
16. Martin P, Aksamija Z, Pop E, Ravaioli U: **Impact of phonon-surface roughness scattering on thermal conductivity of thin Si nanowires.** *Phys Rev Lett* 2009, **102**:125503.
17. Abramson AR, Kim WC, Huxtable ST, Yan HQ, Wu YY, Majumdar A, Tien CL, Yang PD: **Fabrication and characterization of a nanowire/polymer-based nanocomposite for a prototype thermoelectric device.** *J Microelectromech Syst* 2004, **13**:505–513.
18. Haynes CL, Van Duyne RP: **Nanosphere lithography: a versatile nanofabrication tool for studies of size-dependent nanoparticle optics.** *J Phys Chem B* 2001, **105**:5599–5611.
19. Zhong X, Qu YQ, Lin YC, Liao L, Duan XF: **Unveiling the formation pathway of single crystalline porous silicon nanowires.** *ACS Appl Mater Interfaces* 2011, **3**:261–270.
20. Qu Y, Zhou H, Duan X: **Porous silicon nanowires.** *Nanoscale* 2011, **3**:4060–4068.
21. Weisse JM, Lee CH, Kim DR, Zheng X: **Fabrication of flexible and vertical silicon nanowire electronics.** *Nano Lett* 2012, **12**:3339–3343.
22. Garnett E, Yang PD: **Light trapping in silicon nanowire solar cells.** *Nano Lett* 2010, **10**:1082–1087.
23. Qu YQ, Liao L, Li YJ, Zhang H, Huang Y, Duan XF: **Electrically conductive and optically active porous silicon nanowires.** *Nano Lett* 2009, **9**:4539–4543.
24. Weisse JM, Kim DR, Lee CH, Zheng X: **Vertical transfer of uniform silicon nanowire arrays via crack formation.** *Nano Lett* 2011, **11**:1300–1305.
25. Kim J, Han H, Kim YH, Choi S-H, Kim J-C, Lee W: **Au/Ag bilayered metal mesh as a Si etching catalyst for controlled fabrication of Si nanowires.** *ACS Nano* 2011, **5**:3222–3229.
26. Zhang ML, Peng KQ, Fan X, Jie JS, Zhang RQ, Lee ST, Wong NB: **Preparation of large-area uniform silicon nanowires arrays through metal-assisted chemical etching.** *J Phys Chem C* 2008, **112**:4444–4450.
27. Chiappini C, Liu X, Fakhoury JR, Ferrari M: **Biodegradable porous silicon barcode nanowires with defined geometry.** *Adv Funct Mater* 2010, **20**:2231–2239.
28. Panzer MA, Zhang G, Mann D, Hu X, Pop E, Dai H, Goodson KE: **Thermal properties of metal-coated vertically aligned single-wall nanotube arrays.** *J Heat Transfer* 2008, **130**:052401.
29. Asheghi M, Kurabayashi K, Kasnavi R, Goodson KE: **Thermal conduction in doped single-crystal silicon films.** *J Appl Phys* 2002, **91**:5079–5088.
30. Slack GA: **Thermal conductivity of pure and impure silicon, silicon carbide, and diamond.** *J Appl Phys* 1964, **35**:3460–3465.